IOP Publishing Physica Scripta
Phys. Scr. 95 (2020) 045204 (10pp) https://doi.org/10.1088/1402-4896/ab4eb3

High-order rational solutions and rogue wave for the (2 + 1)-dimensional nonlinear Schrödinger equation

Wenhao Liu and Yufeng Zhang

School of Mathematics, China University of Mining and Technology, Xuzhou, Jiangsu, 221116, People's Republic of China

E-mail: zhangyfcumt@163.com

Received 2 August 2019, revised 19 September 2019
Accepted for publication 17 October 2019
Published 11 February 2020

Abstract

In this paper, some exact explicit rational solutions of the (2 + 1)-dimensional nonlinear Schrödinger equation are presented in terms of the Gram determinants by using the bilinear method. The expressions of the fundamental line rogue wave, second-order parallel line rogue wave and third-order parallel line rogue wave all involve determinants whose matrix elements are simple polynomials. These line rogue waves, which all generate from a constant background with line contours and then disappear into the same background, are plotted in the (x, y)-plane. Moreover, we also consider different structures of higher-order rogue waves, and their dynamical behaviors are illustrated in the (x, t)-plane.

Keywords: (2 + 1)-dimensional nonlinear Schrödinger equation, bilinear transformation method, parallel line rogue waves

(Some figures may appear in colour only in the online journal)

1. Introduction

The nonlinear Schrödinger equation (NLS) which was first derived by Zakharov in his study of modulation stability of deep water waves [1], a class of nonlinear systems that can control weak nonlinearity and dispersion wave packet in one-dimensional physical systems, is an important integrable equation. In 1973, Hasegawa and Tappert found that the propagation of optical pulses in optical fibers is controlled by NLS equation [2]. Because of its practical significance, researchers use Schrödinger equation to explain some nonlinear phenomena with high frequency in fields such as particle physics, condensed matter physics, fluids and optics [3–9]. Under this background, it is especially important to solve the soliton solution of NLS equations. It is worth mentioning that analytical vector multipole and vortex soliton solutions of a (2 + 1)-dimensional coupled NLS equation are investigated by Dai [10]. In the same year, hierarchies of Peregrine solution and breather solution are derived in a (2 + 1)-dimensional variable-coefficient NLS equation [11]. Recently, rogue waves (RWs) of NLS equation, a novel type of rational solitary waves, have attracted wide attention of mathematics and physicists. RWs were first observed in deep ocean [12, 13], then, in optical fibres [14] and several other physical settings [15], RWs appeared. A thorough study of RWs can give people a comprehensive understanding of some abstract natural phenomena. A variety of NLS equations including nonlocal systems satisfying parity-time (PT) symmetry have been verified possessing RW solutions [16–18]. For instance, variable-coefficient (2 + 1)-dimensional Heisenberg ferromagnetic spin chain equation [19] and coupled 2D NLS equations [20]. Hence finding the RW of NLS equation is a topic of great significance. In the last decades, a variety of construction methods for RW solution of NLS equation have been established, such as the Hirota's bilinear method [21–23], the Darboux transformation method [24], the inverse scattering method [25]. Generally, it is easy to derive the RWs of (1 + 1)-dimensional NLS equations, but the higher-dimensional ones are not simple. However, in 2012, Yasuhiro Ohta proposed a new method to help us obtain the RW of the high-dimensional Schrödinger equation [26].

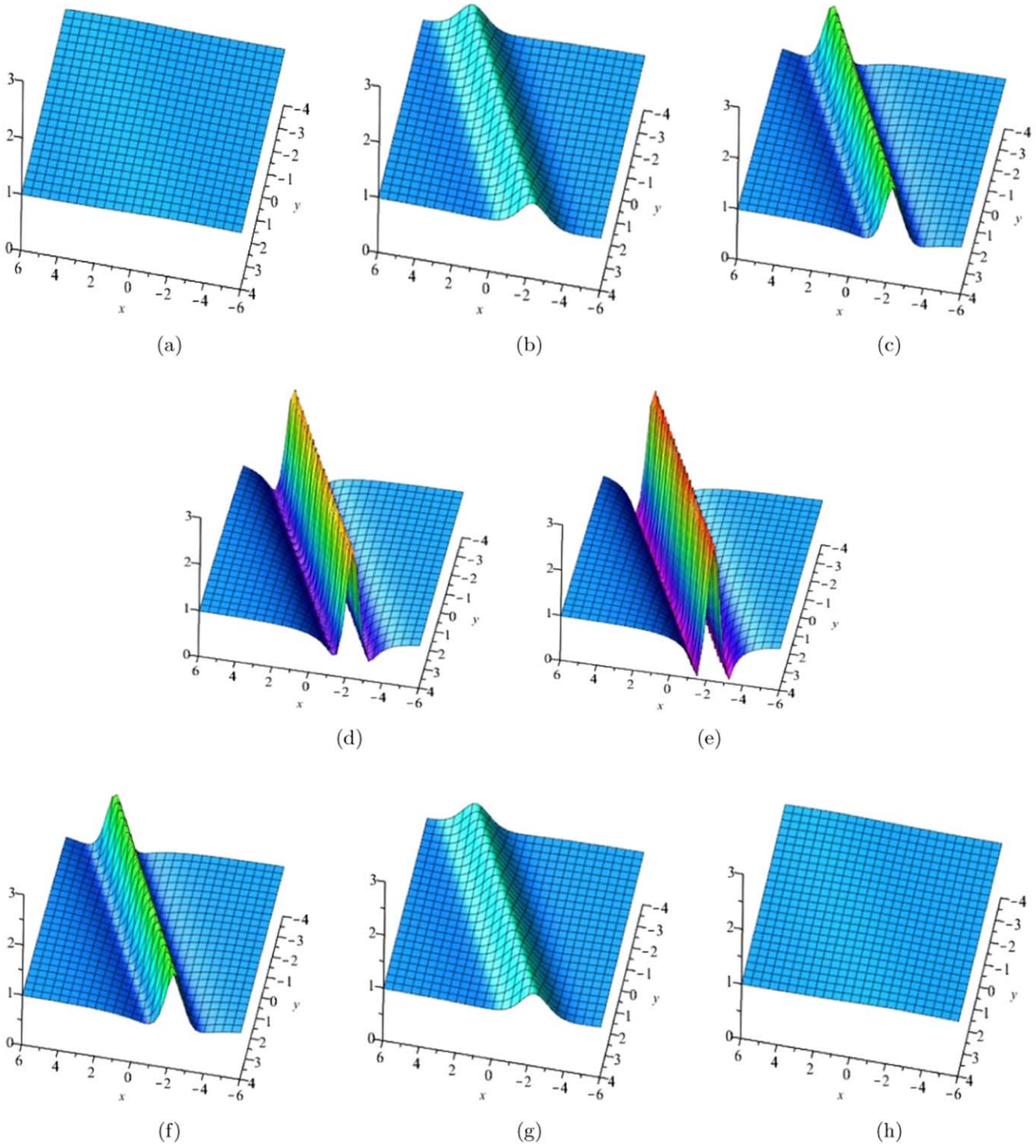

Figure 1. The fundamental line rogue wave (3.3) of equation (1.1) with the parameter $r_1 = 0$, which is plotted in the (x, y)-plane. (a) $t = -4$, (b) $t = -1$, (c) $t = -\frac{1}{2}$, (d) $t = -\frac{1}{6}$, (e) $t = 0$, (f) $t = \frac{1}{2}$, (g) $t = 1$, (h) $t = 4$.

In this paper, we mainly focus on the following (2 + 1)-dimensional NLS

$$\mathrm{i}u_t + u_{x,y} + u\mathcal{P} = 0, \quad \mathcal{P}_y = |u|_x^2, \tag{1.1}$$

where $\mathcal{P}$ is a real function, and u is a complex-valued function, which discussed by Svachan is shown to admit the painlevé property. The bilinear form of the (2 + 1)-dimensional NLS equation has been obtained by Radha and Lakshmanan [27]. The bifurcations and travelling wave solutions of the equation (1.1) are also studied by Wang [28]. Moreover, the general periodic solutions and RW solutions of the (2 + 1)-dimensional NLS equation with the self-induced PT symmetric potential are derived [29]. The main purpose of the present

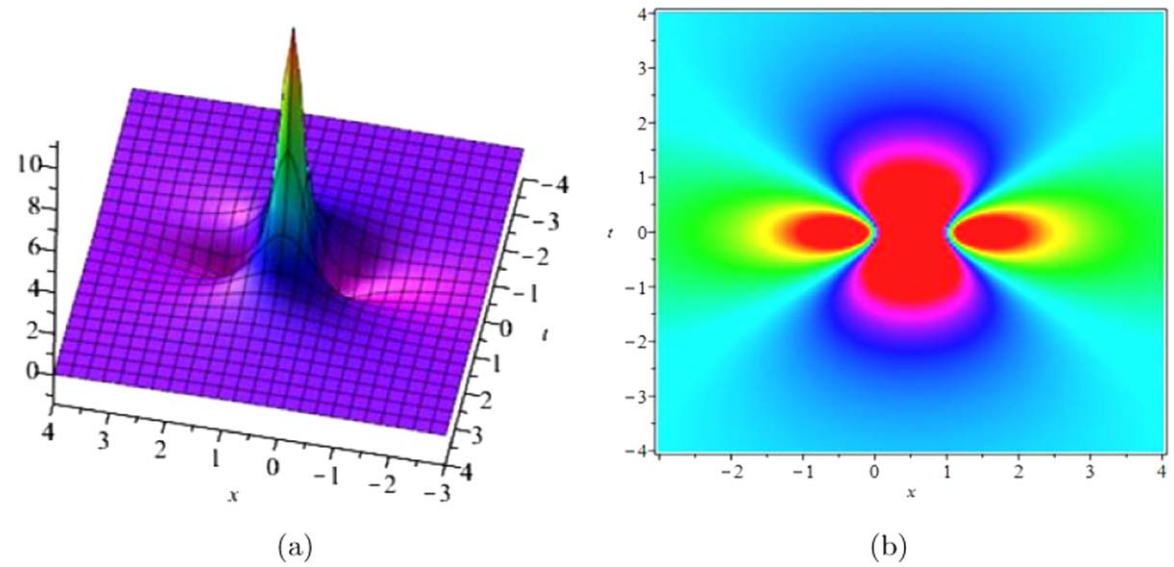

Figure 2. The fundamental rogue wave $\mathcal{P}$ of equation (1.1) with the parameter $r_1 = 0$ and $y = 0$, which is plotted in the (x, t)-plane. (a) three dimensional plot, (b) the density plot.

paper is to study the exact explicit rational solutions of equation (1.1) in terms of the Gram determinants.

The rest of this paper is organised as follows. In section 2, the bilinear form of the (2 + 1)-dimensional NLS is proposed. The explicit rational solutions of the equation (1.1) are also presented in the determinant form based on the results of theorem 1. In section 3, the fundamental-, second-order and third-order line RW are obtained. Especially, the specific formulas of the maximum amplitude and the minimum amplitude of fundamental line RW $|u|$ are given. Furthermore, the dynamic characteristics of these solutions are displayed in figures 1–6 by selecting some special parameters of coefficients. Section 4 contains a conclusion and discussion.

2. RW solutions via determinants of $N \times N$ matrices

In the section, we discuss the general RWs for the (2 + 1)-dimensional NLS. The bilinear forms of equation (1.1)

$$\begin{aligned}(\mathrm{i}D_t + D_xD_y)g \cdot f = 0,\\ (D_y^2 + 1)f \cdot f = gg^*,\end{aligned} \tag{2.1}$$

which are given in [27], can be obtained by the following variable transformation

$$u = \frac{g}{f}, \quad \mathcal{P} = 2(\log f)_{xy}, \tag{2.2}$$

where f and g are the functions with respect to x, y and t, and the operator D is the Hirota's bilinear differential operator defined in [30].

Theorem 1. *The equation (2.2) is the rational solutions of the (2 + 1)-dimensional NLS equation (1.1), where f and g are expressed by the determinants of the N × N matrices*

$$f = \tau_l\,|_{l=0}, \quad g = \tau_l\,|_{l=1}, \tag{2.3}$$

with the matrix τ_1 *can be given by* $\tau_l = \det_{1\leqslant i,j\leqslant N}(\lambda^{(l)}_{2i-1,2j-1})$,

$$\begin{cases}\lambda^{(l)}_{i,j} = \displaystyle\sum_{m=0}^{i}\frac{r_m}{(i-m)!}(p\partial_p + \mu' + l)^{i-m}\sum_{n=0}^{j}\frac{r_n^*}{(j-n)!}(p^*\partial_{p^*} + \mu'^* - l)^{j-n}\frac{1}{p+p^*}\Big|_{p=1},\\ \mu' = \dfrac{y}{p} + p\left[x + \left(-1 + \dfrac{\sqrt{2}}{2}\right)y\right] + \sqrt{2}\,\mathrm{i}p^2t.\end{cases} \tag{2.4}$$

Here i, j are arbitrary positive integers, $\mathrm{r_m}$ and $\mathrm{r_n}$ are arbitrary complex constants.

Lemma 1. *The bilinear equation (2.1) has the Gram determinant solutions* $\tau_l = \det_{1\leqslant i,j\leqslant N}(\lambda^{(l)}_{i,j})$ *in the KP hierarchy*

$$\begin{aligned}(D_{x_1}^2 + D_{x_2})\tau_{l+1}\cdot\tau_l = 0,\\ (D_{x_1}D_{x_{-1}} - 2)\tau_l\cdot\tau_l = -2\tau_{l+1}\cdot\tau_l.\end{aligned} \tag{2.5}$$

Here the matrix element as follows

$$\begin{aligned}\lambda'^{(l)}_{i,j} = &\sum_{m=0}^{i}\frac{r_m}{(i-m)!}(p\partial_p + \mu' + l)^{i-m}\\ &\times\sum_{n=0}^{j}\frac{h_n}{(j-n)!}(q\partial_q + \nu' - l)^{j-n}\frac{1}{p+q},\end{aligned} \tag{2.6}$$

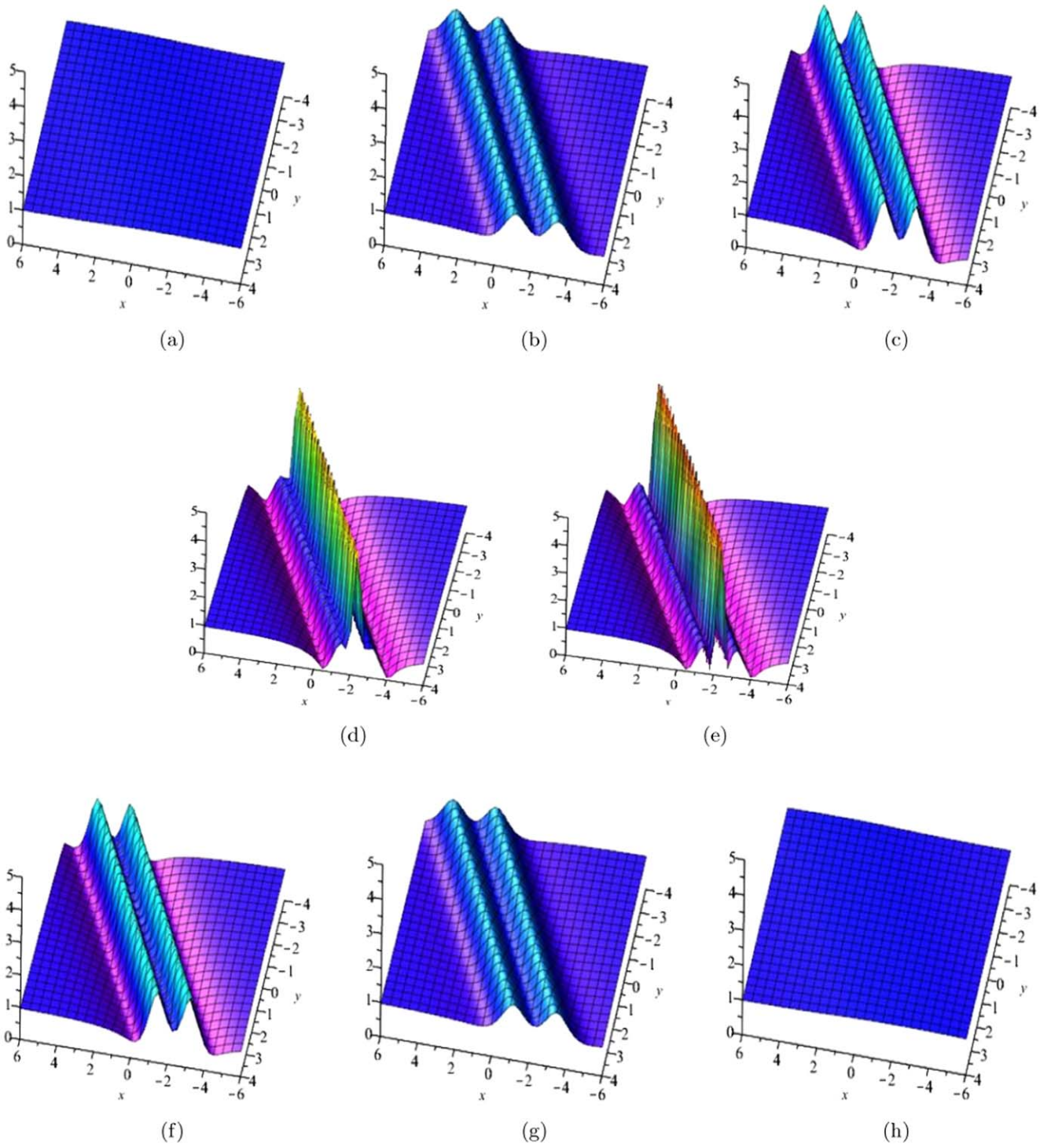

Figure 3. The second-order parallel line rogue wave $|u|$ of equation (1.1) with the parameter $r_1 = 0$ and $r_3 = -\frac{1}{12}$, which is plotted in the (x, y)-plane. (a) $t = -4$, (b) $t = -1$, (c) $t = -\frac{1}{2}$, (d) $t = -\frac{1}{20}$, (e) $t = 0$, (f) $t = \frac{1}{2}$, (g) $t = 1$, (h) $t = 4$.

where

$$\mu' = px_1 + 2p^2x_2 - \frac{1}{p}x_{-1},$$
$$\nu' = qx_1 - 2q^2x_2 - \frac{1}{q}x_{-1}, \tag{2.7}$$

p, q, r_m, h_n are arbitrary complex constants, and i, j, N are arbitrary positive integers.

The proof of lemma 1 has been given by [26]. Using the lemma 1, we can get the results of theorem 1 [26]. Especially, the bilinear equation (2.1) can be transformed into the bilinear equation (2.5) by selecting the corresponding independent

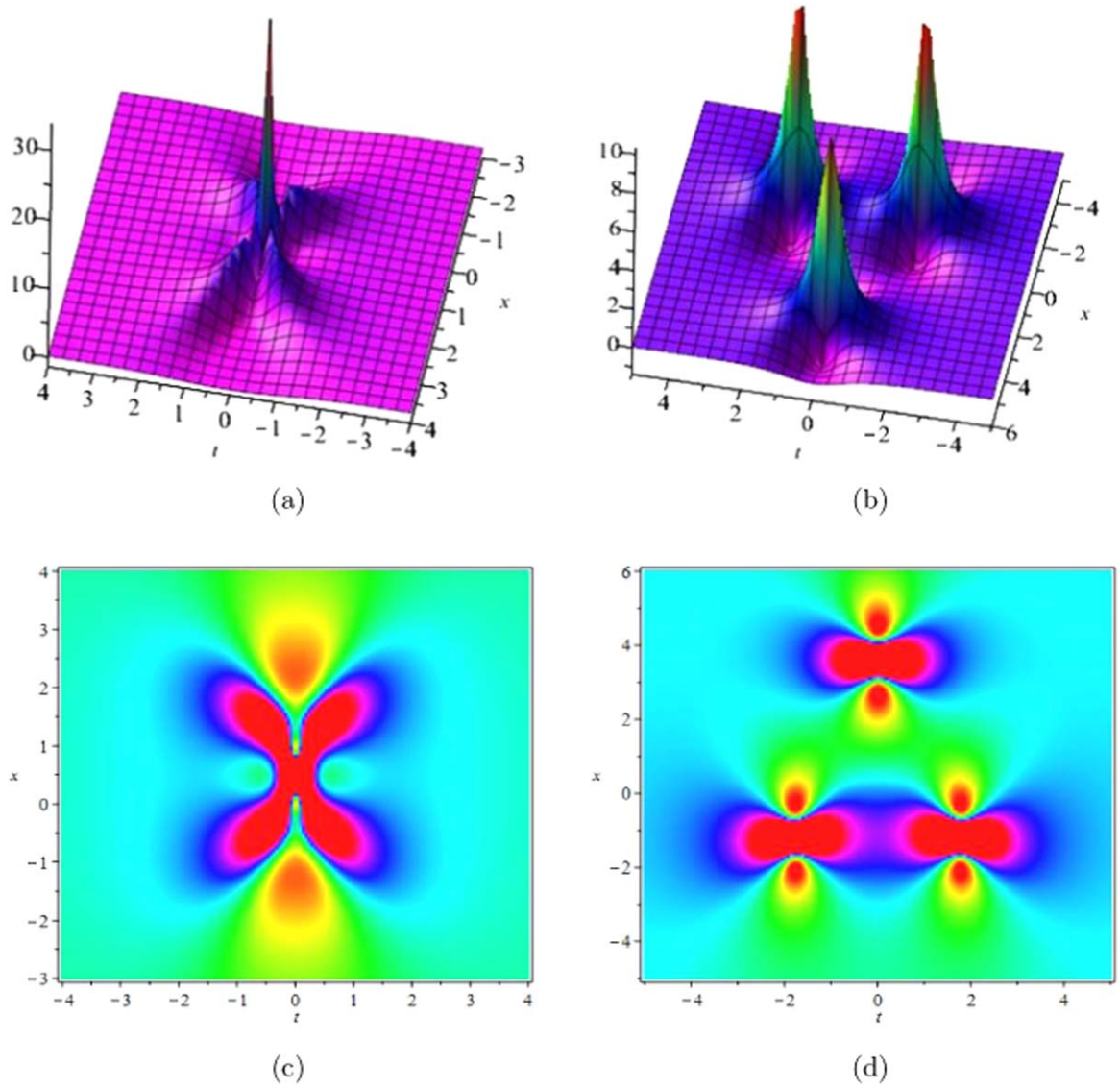

Figure 4. The second-order rogue wave $\mathcal{P}$ of equation (1.1) with the parameter $r_1 = 0$ and $y = 0$, which is plotted in the (x, t)-plane. (a), (c) $r_3 = -\frac{1}{12}$, (b), (d) $r_3 = 10$.

variables $x_{-1} = -y$, $x_1 = x + (-1 + \frac{\sqrt{2}}{2})y$, $x_2 = \frac{\sqrt{2}}{2}it$. Thus it can be seen that we can obtain the rational solutions of the (2 + 1)-dimensional NLS (1.1) from the solutions of equation (2.5) by utilizing the gauge freedom of τ_l. The similar proof of the theorem 1 has been provided in [31], so we omit it here. Next we will discuss several explicit formulas of RW solutions of equation (2.5) from theorem 1. But before that, we take $r_0 = 1$, $r_2 = r_4 = r_6 = \cdots = 0$ without loss of generality, and retain only r_3, r_5, r_7, $\cdots$. This facilitates our next calculations.

3. Dynamics of RWs of the (2 + 1)-dimensional NLS equation

In the section, we examine the dynamics of the (2 + 1)-dimensional NLS

3.1. Fundamental RW solutions

By observing the results in the theorem 1, the rational solutions can be written when we take $N = 1$

$$u = \frac{\lambda_{11}^{(1)}}{\lambda_{11}^{(0)}}, \quad \mathcal{P} = 2(\log \lambda_{11}^{(0)})_{xy}, \tag{3.1}$$

where

$$\begin{aligned}\lambda_{11}^{(0)} &= \sum_{m=0}^{1} \frac{r_m}{(1-m)!}(p\partial_p + \mu')^{1-m} \\ &\quad \times \sum_{n=0}^{1} \frac{h_n}{(1-n)!}(q\partial_q + \nu')^{1-n}\frac{1}{p+q} \\ &= (p\partial_p + \mu' + r_1)(q\partial_q + \nu' + h_1)\frac{1}{p+q}\end{aligned}$$

$$= \frac{1}{p+q}\left[\left(\mu' - \frac{p}{p+q} + r_1\right)\left(\nu' - \frac{q}{p+q} + h_1\right) + \frac{pq}{(p+q)^2}\right],$$

$$\lambda_{11}^{(1)} = \sum_{m=0}^{1} \frac{r_m}{(1-m)!}(p\partial_p + \mu' + 1)^{1-m} \times \sum_{n=0}^{1} \frac{h_n}{(1-n)!}(q\partial_q + \nu' - 1)^{1-n}\frac{1}{p+q}$$
$$= (p\partial_p + \mu' + r_1 + 1)(q\partial_q + \nu' + h_1 - 1)\frac{1}{p+q}$$
$$= \frac{1}{p+q}\left[\left(\mu' - \frac{p}{p+q} + r_1 + 1\right)\left(\nu' - \frac{q}{p+q} + h_1 - 1\right) + \frac{pq}{(p+q)^2}\right], \tag{3.2}$$

in which $p = q = 1$ and r_1, h_1 are all freely complex constant. Therefore, the exact expression of fundamental RW can be given as

$$u = 1 - \frac{8\sqrt{2}\,\mathrm{i}t + 4}{(2x + \sqrt{2}y - 1)^2 + 8t^2 + 1},$$
$$\mathcal{P} = \frac{8\sqrt{2}}{(2x + \sqrt{2}y - 1)^2 + 8t^2 + 1} - \frac{64\left(\frac{\sqrt{2}}{2}y^2 + 2yx - y + \sqrt{2}x^2 - \sqrt{2}x + \frac{\sqrt{2}}{4}\right)}{[(2x + \sqrt{2}y - 1)^2 + 8t^2 + 1]^2}. \tag{3.3}$$

It is not hard to analyse that the modulus $|u|$ of equation (3.1) has three extreme lines as follows

$$L_1\colon\ y = -\sqrt{2}x + \frac{\sqrt{2}}{2},$$
$$L_2\colon\ y = -\sqrt{2}x + \frac{\sqrt{2}}{2} + \frac{\sqrt{2}}{2}\sqrt{24t^2 + 3},$$
$$L_3\colon\ y = -\sqrt{2}x + \frac{\sqrt{2}}{2} - \frac{\sqrt{2}}{2}\sqrt{24t^2 + 3}. \tag{3.4}$$

Based on this, the maximum amplitude and the minimum amplitude of $|u|$ can be derived, respectively, by solving values of special significance, read

$$|u|_{\max} = |u||_{L_1} = \sqrt{1 + \frac{8}{8t^2 + 1}},$$
$$|u|_{\min} = |u||_{L_2} = |u||_{L_3} = \sqrt{1 - \frac{1}{8t^2 + 1}}. \tag{3.5}$$

It has been proved from the above equation that $|u|_{\max} \to |u|_{\min} = 1$ when $t \to \pm\infty$, which tell us that the rational solution (3.3) approaches a constant background with $|t|$ tending to infinity. Understanding in this background is what we call the line RW. As shown in figure 1, with the value of time t increasing, amplitude of the line RW increases until reaches its maximum 3 at $t = 0$. Taking $t = 0$ as the demarcation point, with the value of time t continues to increases, amplitude of the line RW gradually decreases. Ultimately, the wave approaches the constant background when $t \gg 0$. Figure 2 presents the fundamental RW $\mathcal{P}$ of equation (3.3) in the (x, t)-plane. It is not difficult to see these RWs have different dynamics in different planes. In particular, the Nth-order RWs consist of $\frac{N(N+1)}{2}$ localized waves, which have the characteristics of $(1 + 1)$ dimensional RWs.

3.2. High-order RW solutions

The results of theorem 1 tell us that we can consider the Nth-order RWs for the $(2 + 1)$-dimensional NLS (1.1) by selecting an arbitrary given value of N. Thus the explicit form of the second-order RW solution can be written in the circumstances of $N = 2$ as

$$u = \frac{\begin{vmatrix} \lambda_{11}^{(1)} & \lambda_{13}^{(1)} \\ \lambda_{31}^{(1)} & \lambda_{33}^{(1)} \end{vmatrix}}{\begin{vmatrix} \lambda_{11}^{(0)} & \lambda_{13}^{(0)} \\ \lambda_{31}^{(0)} & \lambda_{33}^{(0)} \end{vmatrix}}, \quad \mathcal{P} = 2\left(\log \begin{vmatrix} \lambda_{11}^{(0)} & \lambda_{13}^{(0)} \\ \lambda_{31}^{(0)} & \lambda_{33}^{(0)} \end{vmatrix}\right)_{xy}. \tag{3.6}$$

In section 2, we have pointed out that $r_0 = 1$, $r_2 = 0$, and r_3 is arbitrary complex constants. Here we just letting $r_1 = 0$ in equation (3.6), the second-order RW solution admits the expansion

$$u = 1 - \frac{G_2}{F_2}, \quad \mathcal{P} = 2(\log F_2)_{xy}, \tag{3.7}$$

where

$$G_2 = -\frac{1}{32}x - \frac{\sqrt{2}}{64}y + \frac{1}{8}r_3x + \frac{1}{16}y^2x^2 - \frac{1}{16}y^2x - \frac{1}{4}xt^2 - \frac{\sqrt{2}}{96}y^3 + \frac{1}{8}y^2t^2 + \frac{1}{4}x^2t^2 + \frac{\sqrt{2}}{4}yxt^2 + \frac{1}{6}\mathrm{i}tx^3y + \frac{1}{4}\mathrm{i}r_3ty + \frac{\sqrt{2}}{12}\mathrm{i}t^3y^3 + \frac{\sqrt{2}}{96}\mathrm{i}ty^4 + \frac{1}{3}\mathrm{i}t^3xy + \frac{1}{12}\mathrm{i}txy^3 + \frac{\sqrt{2}}{6}\mathrm{i}t^3x^2 + \frac{\sqrt{2}}{24}\mathrm{i}tx^4 + \frac{\sqrt{2}}{16}\mathrm{i}xt + \frac{\sqrt{2}}{16}yx - \frac{\sqrt{2}}{16}yx^2 - \frac{\sqrt{2}}{8}yt^2 + \frac{\sqrt{2}}{24}yx^3 + \frac{\sqrt{2}}{48}y^3x + \frac{\sqrt{2}}{16}r_3y - \frac{1}{16}r_3 + \frac{1}{32}y^2 - \frac{1}{24}x^3 + \frac{1}{192}y^4 + \frac{1}{48}x^4 + \frac{5}{12}t^4 + \frac{1}{4}t^2 + \frac{1}{16}x^2 - \frac{\sqrt{2}}{8}\mathrm{i}xty^2 + \frac{\sqrt{2}}{6}\mathrm{i}t^5 + \frac{\sqrt{2}}{12}\mathrm{i}t^3 + \frac{1}{16}\mathrm{i}yt - \frac{\sqrt{2}}{6}\mathrm{i}t^3x - \frac{1}{4}\mathrm{i}yx^2t - \frac{\sqrt{2}}{12}\mathrm{i}tx^3 - \frac{\sqrt{2}}{8}r_3\mathrm{i}t - \frac{1}{24}\mathrm{i}y^3t - \frac{1}{16}\mathrm{i}y^3t - \frac{1}{6}\mathrm{i}yt^3 + \frac{\sqrt{2}}{4}r_3\mathrm{i}xt + \frac{\sqrt{2}}{8}\mathrm{i}ty^2x^2,$$

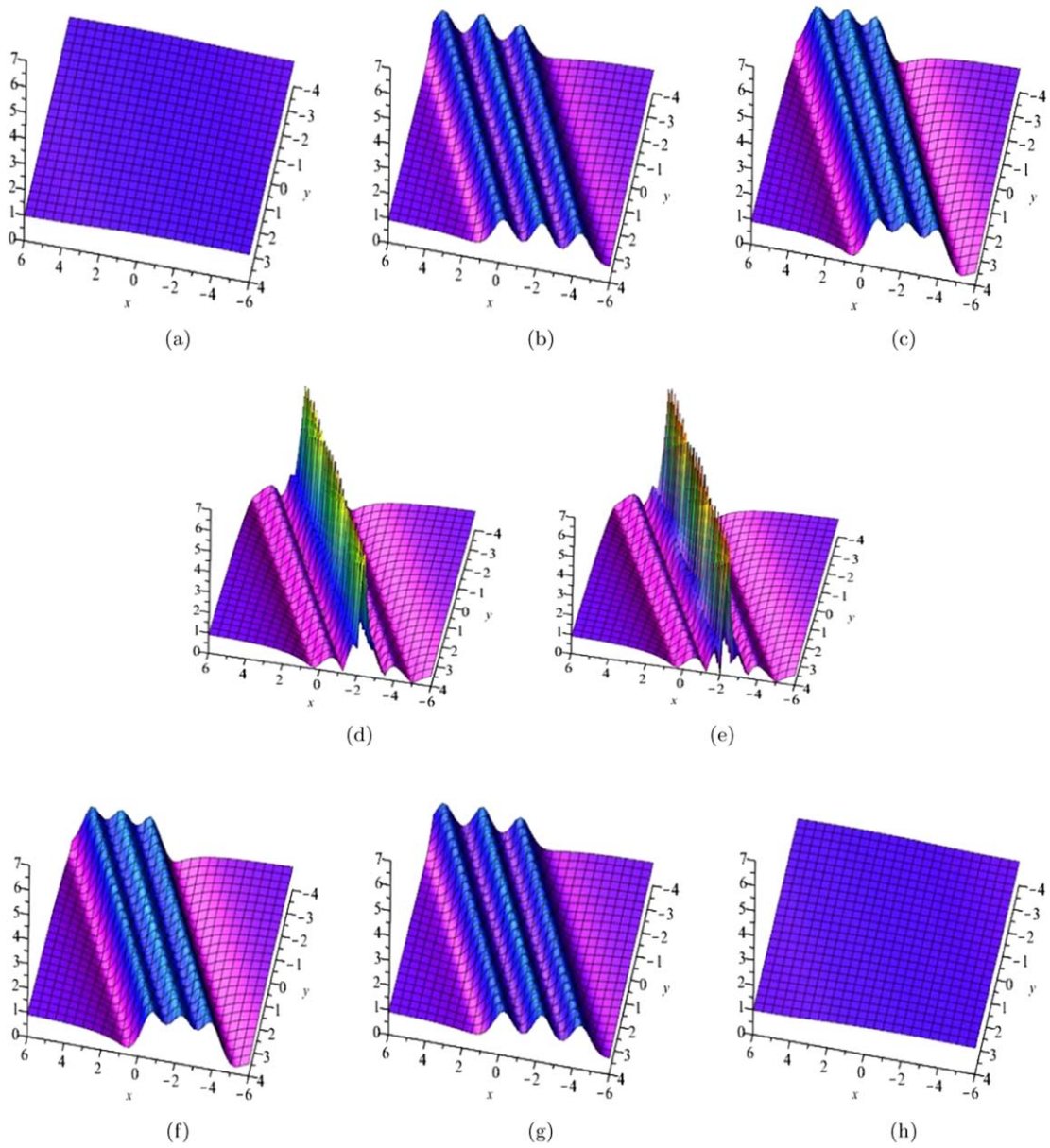

Figure 5. The third-order parallel line rogue wave $|u|$ of equation (1.1) with the parameter $r_1 = 0$, $r_3 = -\frac{1}{12}$ and $r_5 = -\frac{1}{240}$, which is plotted in the (x, y)-plane. (a) $t = -4$, (b) $t = -1$, (c) $t = -\frac{1}{2}$, (d) $t = -\frac{1}{40}$, (e) $t = 0$, (f) $t = \frac{1}{2}$, (g) $t = 1$, (h) $t = 4$.

$$
\begin{aligned}
F_2 = {} & -\frac{1}{64}x + \frac{1}{32}x^2 + \frac{1}{64}y^2 - \frac{1}{32}x^3 + \frac{1}{128}y^4 + \frac{1}{32}x^4 \\
& + \frac{5}{24}t^4 + \frac{1}{16}t^2 - \frac{3}{64}y^2x + \frac{1}{16}xt^2 + \frac{3}{32}y^2x^2 \\
& + \frac{\sqrt{2}}{24}y^3xt^2 + \frac{\sqrt{2}}{8}r_3yt^2 + \frac{\sqrt{2}}{12}yxt^4 + \frac{\sqrt{2}}{12}yx^3t^2 \\
& - \frac{\sqrt{2}}{16}r_3yx^2 + \frac{\sqrt{2}}{16}r_3xy - \frac{\sqrt{2}}{8}yx^2t^2 - \frac{1}{8}r_3t^2 + \frac{1}{18}t^6 \\
& + \frac{1}{1152}y^6 + \frac{1}{144}x^6 - \frac{1}{48}x^5 - \frac{1}{16}r_3y^2x + \frac{1}{8}y^2x^2t^2 \\
& + \frac{1}{4}r_3xt^2 - \frac{1}{8}y^2xt^2 + \frac{1}{12}x^2t^4 + \frac{1}{24}x^4t^2 - \frac{1}{24}r_3x^3 \\
& + \frac{1}{24}y^2t^4 + \frac{5}{96}y^2x^4 + \frac{5}{192}y^4x^2 - \frac{5}{48}y^2x^3 - \frac{5}{192}y^4x \\
& + \frac{1}{32}r_3y^2 - \frac{1}{12}xt^4 - \frac{1}{12}x^3t^2 + \frac{1}{16}r_3x^2 - \frac{\sqrt{2}}{128}y \\
& - \frac{\sqrt{2}}{128}y^3 + \frac{\sqrt{2}}{32}yt^2 + \frac{\sqrt{2}}{32}yx + \frac{\sqrt{2}}{16}yx^3 + \frac{\sqrt{2}}{32}y^3x \\
& - \frac{3\sqrt{2}}{64}yx^2 + \frac{5\sqrt{2}}{144}y^3x^3 + \frac{\sqrt{2}}{192}y^5x - \frac{\sqrt{2}}{96}r_3y^3
\end{aligned}
$$

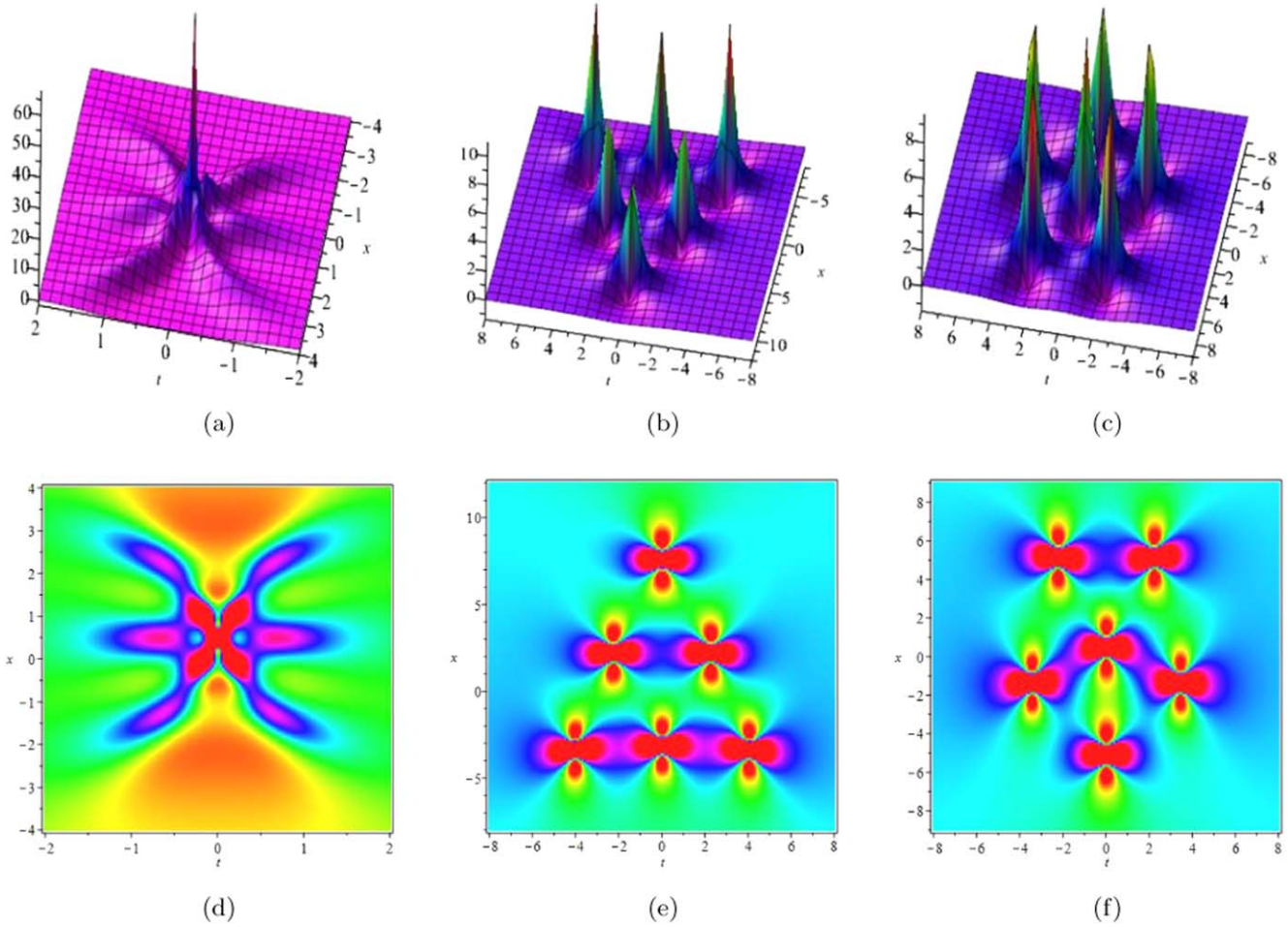

Figure 6. The third-order rogue wave $\mathcal{P}$ of equation (1.1) with the parameter $r_1 = 0$ and $y = 0$, which is plotted in the (x, t)-plane. (a), (c) $r_3 = -\frac{1}{12}$ and $r_5 = -\frac{1}{240}$, (b), (d) $r_3 = 20$ and $r_5 = 0$, (c), (f) $r_3 = 0$ and $r_5 = 120$.

$$+\frac{\sqrt{2}}{48}yx^5 - \frac{\sqrt{2}}{24}yt^4 - \frac{5\sqrt{2}}{96}yx^4 - \frac{5\sqrt{2}}{96}y^3x^2 - \frac{\sqrt{2}}{48}y^3t^2 + \frac{1}{16}r_3^2 - \frac{\sqrt{2}}{384}y^5 + \frac{1}{256}. \tag{3.8}$$

The corresponding second-order parallel line RW $|u|$ and second-order RW $\mathcal{P}$ are shown in figures 3 and 4, respectively. Figure 3 displays the changing dynamic of the second-order parallel line RW over time t. It can be seen that when two parallel traveling waves are generated by a constant background in the (x, y)-plane, the intersection of their regions produces a higher amplitude (As shown in figure 3(b)). And then when the time t equals zero, the superposition of two parallel traveling waves produces a maximum main peak with an amplitude of 5 and several lower peaks (see figure 3(e)). Ultimately, the attenuation of two parallel RW returns to a constant background. Figure 4(a) depicts the fundamental pattern generated by interaction of these three RWs, and figure 4(b) present the triangular pattern.

This is what we will do: further discussion on the case of $N = 3$ in theorem 1. The third-order RW solution has the following forms

$$u = \frac{\begin{vmatrix} \lambda_{11}^{(1)} & \lambda_{13}^{(1)} & \lambda_{15}^{(1)} \\ \lambda_{31}^{(1)} & \lambda_{33}^{(1)} & \lambda_{35}^{(1)} \\ \lambda_{51}^{(1)} & \lambda_{53}^{(1)} & \lambda_{55}^{(1)} \end{vmatrix}}{\begin{vmatrix} \lambda_{11}^{(0)} & \lambda_{13}^{(0)} & \lambda_{15}^{(0)} \\ \lambda_{31}^{(0)} & \lambda_{33}^{(0)} & \lambda_{35}^{(0)} \\ \lambda_{51}^{(0)} & \lambda_{53}^{(0)} & \lambda_{55}^{(0)} \end{vmatrix}}, \quad \mathcal{P} = 2\left(\log \begin{vmatrix} \lambda_{11}^{(0)} & \lambda_{13}^{(0)} & \lambda_{15}^{(0)} \\ \lambda_{31}^{(0)} & \lambda_{33}^{(0)} & \lambda_{35}^{(0)} \\ \lambda_{51}^{(0)} & \lambda_{53}^{(0)} & \lambda_{55}^{(0)} \end{vmatrix}\right)_{xy}. \tag{3.9}$$

We no longer give the expression of the third-order RW solution because they are too lengthy. With the selection of the parameters

$$r_0 = 1, \quad r_1 = 0, \quad r_2 = 0, \quad r_3 = -\frac{1}{12}, \quad r_4 = 0, \quad r_5 = -\frac{1}{240}, \tag{3.10}$$

the third-order parallel line RW $|u|$ is obtained and plotted in figure 5. We get more complex three-dimensional plot than the second-order parallel line RW (3.7). The third-order parallel line RW consists of three independent fundamental RWs in the

(x, y)-plane. We noticed that the third-order parallel line RW and the second-order parallel line RW have similar dynamic characteristics as time t goes by. When $t = 0$, the superposition of three parallel traveling waves produces a maximum peak with an amplitude of 7. For figure 6, the third-order RW of equation (1.1) is composed by 6 fundamental localized waves the (x, t)-plane. The third-order RW also has three basic patterns: the fundamental pattern, the triangular pattern and the ring pattern.

4. Conclusion and discussion

In this paper, we investigated the $(2 + 1)$-dimensional NLS by utilizing the bilinear transformation method. The general formula for the Nth-order RW solutions of the equation (1.1) are constructed based on the results of theorem 1, in which these solutions are expressed explicitly in terms of determinants. The corresponding fundamental parallel line RW $|u|$ in the (x, y)-plane and fundamental RW $\mathcal{P}$ in the (x, t)-plane are given in equation (3.3). The dynamic characteristics of these solutions are analyzed, and we can easy to know that, with the value of time t increasing, amplitude of the line RW increases until reaches its maximum at $t = 0$. Finally, these waves approach the constant background when $t \gg 0$. Furthermore, we observed that the second-order RW and the third-order RW consist of two parallel line RWs and three parallel line RWs, respectively (see figures 3 and 5). In addition, the dynamics of these line RWs in the (x, t)-plane are shown in figures 2, 4, 6. It is worth noting that the Nth-order RW consists of $\frac{N(N+1)}{2}$ localized waves, which have the characteristics of $(1 + 1)$ dimensional RWs. Our results reveal a range of interesting and complicated dynamics, and we hope they can help explain some special phenomena in the filed of mathematical physics and engineering.

Acknowledgments

This work is supported by the Fundamental Research Funds for the Central University (No. 2017XKZD11).

Conflicts of interest

The authors declare that they have no conflicts of interest.

ORCID iDs

Wenhao Liu https://orcid.org/0000-0002-0088-6433

References

[1] Zakharov V E 1968 Stability of periodic waves of finite amplitude on the surface of a deep fluid *J. Appl. Mech. Tech. Phys.* **9** 190–4

[2] Hasegawa A and Tappert F 1973 Transmission of stationary nonlinear optical pulses in dispersive dielectric fibers: I. Anomalous dispersion *Appl. Phys. Lett.* **23** 142–4

[3] Razavy M 1978 Hamilton's principal function for the Brownian motion of a particle and the Schrödinger–Langevin equation *Can. J. Phys.* **56** 311–20

[4] Zhang Y 2019 Similarity solutions and the computation formulas of a nonlinear fractional-order generalized heat equation *Mod. Phys. Lett.* B 1950122

[5] Fedele R and Schamel H 2002 Solitary waves in the Madelung's fluid: Connection between the nonlinear Schrödinger equation and the Korteweg–de Vries equation *Eur. Phys. J.* B **27** 313–20

[6] Wang Y Y *et al* 2017 Exact vector multipole and vortex solitons in the media with spatially modulated cubic-quintic nonlinearity *Nonlinear Dyn.* **90** 1269–75

[7] Ding D J, Jin D Q and Dai C Q 2017 Analytical solutions of differential-difference sine-Gordon equation *Therm. Sci.* **21** 1701–5

[8] Tian S F 2017 Initial-boundary value problems for the general coupled nonlinear Schrödinger equation on the interval via the Fokas method *J. Differ. Equ.* **262** 506–58

[9] Dai C Q *et al* 2017 Dynamics of light bullets in inhomogeneous cubic-quintic-septimal nonlinear media with $\mathcal{PT}$-symmetric potentials *Nonlinear Dyn.* **87** 1675–83

[10] Dai C Q *et al* 2017 Vector multipole and vortex solitons in two-dimensional Kerr media *Nonlinear Dyn.* **88** 2629–35

[11] Dai C Q *et al* 2017 Two-dimensional localized Peregrine solution and breather excited in a variable-coefficient nonlinear Schrödinger equation with partial nonlocality *Nonlinear Dyn.* **88** 1373–83

[12] Osborne A R 2010 *Nonlinear Ocean Waves and The Inverse Scattering Transform* (New York: Academic)

[13] Pelinovsky Efim and Kharif Christian 2008 *Extreme Ocean Waves* (Berlin: Springer)

[14] Kibler B *et al* 2010 The Peregrine soliton in nonlinear fibre optics *Nat. Phys.* **6** 790

[15] He J *et al* 2014 Theoretical and experimental evidence of non-symmetric doubly localized rogue waves *Proc. R. Soc.* A **470** 20140318

[16] Rao J *et al* 2017 Rogue-wave solutions of the Zakharov equation *Theor. Math. Phys.* **193** 1783–800

[17] Dubard P and Matveev V B 2013 Multi-rogue waves solutions: from the NLS to the KP-I equation *Nonlinearity* **26** R93

[18] Zha Q L 2013 Rogue waves and rational solutions of a (3+1)-dimensional nonlinear evolution equation *Phys. Lett.* A **377** 3021–6

[19] Li B Q and Ma Y L 2019 Characteristics of rogue waves for a $(2 + 1)$-dimensional Heisenberg ferromagnetic spin chain system *J. Magn. Magn. Mater.* **474** 537–43

[20] Cao Y, Malomed B A and He J 2018 Two $(2 + 1)$-dimensional integrable nonlocal nonlinear Schrödinger equations: breather, rational and semi-rational solutions *Chaos Solitons Fractals* **114** 99–107

[21] Liu W J *et al* 2008 Soliton interaction in the higher-order nonlinear Schrödinger equation investigated with Hirota's bilinear method *Phys. Rev.* E **77** 066605

[22] Liu W, Zhang Y and Shi D 2019 Lump waves, solitary waves and interaction phenomena to the $(2 + 1)$-dimensional Konopelchenko–Dubrovsky equation *Phys. Lett.* A **383** 97–102

[23] Jia T T, Chai Y and Hao H Q 2016 Multisoliton solutions and breathers for the coupled nonlinear Schrödinger equations via the Hirota method *Math. Problems Eng.* **2016** 1741245

[24] Guo B, Ling L and Liu Q P 2013 High-order solutions and generalized Darboux transformations of derivative nonlinear Schrödinger equations *Stud. Appl. Math.* **130** 317–44

[25] Prinari B, Ablowitz M J and Biondini G 2006 Inverse scattering transform for the vector nonlinear Schrödinger equation with nonvanishing boundary conditions *J. Math. Phys.* **47** 063508
[26] Ohta Y and Yang J 2012 General high-order rogue waves and their dynamics in the nonlinear Schrödinger equation *Proc. R. Soc.* A **468** 1716–40
[27] Radha R and Lakshmanan M 1994 Singularity structure analysis and bilinear form of a (2 + 1) dimensional nonlinear Schrodinger (NLS) equation *Inverse Problems* **10** L29
[28] Wang J, Chen L and Liu C 2014 Bifurcations and travelling wave solutions of a (2 + 1)-dimensional nonlinear Schrödinger equation *Appl. Math. Comput.* **249** 76–80
[29] Liu Y K and Li B 2017 Rogue waves in the (2 + 1)-dimensional nonlinear Schrödinger equation with a parity-time-symmetric potential *Chin. Phys. Lett.* **34** 010202
[30] Hirota R 2004 *The Direct Method in Soliton Theory* (Cambridge: Cambridge University Press)
[31] Liu Y B *et al* 2016 Parallel line rogue waves of the third-type Davey–Stewartson equation *Rom. Rep. Phys.* **68** 1425–46